Efficient Control of Stochastic Switching via Spin Pumping in Antiferromagnetic Structures

Yuriy G. Semenov[1] and Ki Wook Kim[1,2,*]

[1] *Department of Electrical and Computer Engineering, North Carolina State University, Raleigh, North Carolina 27695, USA*

[2] *Department of Physics, North Carolina State University, Raleigh, North Carolina 27695, USA*

(Received 5 February 2020; revised manuscript received 20 May 2020; accepted 3 June 2020; published 26 June 2020)

Electrically controlled switching in an antiferromagnet (AFM), utilizing a currentless mechanism, is theoretically examined at finite temperatures. The structure consists of a metallic AFM with biaxial magnetic anisotropy sandwiched between a ferromagnetic spin filter and a semiconductor Schottky junction in a two-terminal pillar configuration. The calculations show that the torque necessary for the desired 90° rotation of the Néel vector between two easy axes can be provided efficiently by pumping spin-polarized electrons into and out of the AFM through the metallic ferromagnetic layer. Consideration of thermal fluctuations illustrates the stochastic nature of the switching, whose probability distribution can be tailored by the electrical signal pulse as well as by the device dimensions. Detection of the Néel-vector state following this rotation may also be achieved straightforwardly via the large anisotropic magnetoresistance of the biaxial antiferromagnetic material. These properties, along with an ultrafast switching speed and a low energy requirement, are expected to be well suited for applications in nonvolatile memory and probabilistic computing.

DOI: 10.1103/PhysRevApplied.13.064065

I. INTRODUCTION

Since the discovery of giant magnetoresistance in magnetic heterostructures [1,2], the main focus of spin-based electronics, or spintronics, has been on magnetically ordered materials. The next breakthrough in the field was marked by the prediction and realization of spin-transfer torque (STT) in ferromagnetic nanostructures, where the magnetization can be modulated by a spin-polarized electrical current without the application of external magnetic fields [3,4]. An alternative mechanism of magnetization control was achieved subsequently by using spin-orbit torque (SOT) in a bilayer combination with a strongly spin-orbit-coupled material such as a nonmagnetic heavy metal [5]. In this process, a spin current induced in the adjacent spin-orbit-coupled layer via the spin Hall effect provides the necessary spin interactions at the interface.

Antiferromagnets (AFMs) have only recently been recognized as active spintronic materials with ultrafast dynamics [6–8]. Similarly to ferromagnets (FMs), AFMs inherently possess magnetic properties that are highly desirable for information processing, such as the ability to encode bits with (quasi)stable states of the Néel vector **L**. Manipulation of **L** can also be realized in a manner akin to the use of STT or SOT in FMs [8–10]. In both processes (i.e., SOT and STT), an electrical current mediates two types of torque, namely, antidamping and fieldlike torques. While the former (i.e., the antidamping term) is active throughout the duration of the applied input current as in the case of FMs, the latter impacts the Néel-vector dynamics in a manner proportional to the rate of change of the induced effective field (and thus the time derivative of the current). This is the reason why the fieldlike term has not been considered particularly capable of switching the Néel vector between stable states. As such, the antidamping torque has remained the primary mechanism for achieving oscillation or rotation of the Néel vector. Note, however, that antidamping via SOT or STT also requires an electrical current flow of large magnitude. The resulting energy consumption is generally much higher than the level actually needed to overcome the potential barrier separating the stable states. This inefficiency can be explained by the relativistic origin (in the case of SOT) or the $\hbar/2$ limitation on the angular-momentum transfer of each spin-polarized electron (in the case of STT).

An alternative mechanism based on the nonrelativistic (and thus strong) exchange field was proposed very recently, operating through electron-spin accumulation in a spin-capacitor structure to obviate the restrictions imposed on the transient spin-angular-momentum transfer [11]. Spins pumped into the AFM via charging and discharging of spin-filtered electrons provide the necessary effective

*kwk@ncsu.edu

field, inducing rotation of the Néel vector around it. The advantage derives from the relatively long electron spin relaxation time in AFMs. The resulting extended exposure to the exchange field leads to an effective angular-momentum transfer per electron much larger than that obtained with the STT (i.e., $\hbar/2$). This, combined with the absence of an electrical current flow, can drastically reduce the energy requirement for reversal of the Néel vector. Ironically, one major limitation of the spin-pumping approach is the very use of a capacitor structure for spin accumulation (i.e., no current flow), which, at the same time, restricts detection via magnetoresistance. Furthermore, the 180° switching between the two stable orientations of the Néel vector can only be achieved in a nonselective manner, leaving the state of the AFM macroscopically indistinguishable.

In this paper, the concept of the spin-pumping torque is theoretically explored for a two-terminal AFM structure that can overcome the limitations discussed above while maintaining the advantages at the same time. The study utilizes an additional magnetic anisotropy that breaks the uniaxial symmetry commonly assumed when the 180° reversal of the Néel vector is considered. Specifically, the results for antiferromagnetic materials with biaxial anisotropy illustrate the feasibility of uniquely determining the final state along with electrical detection via anisotropic magnetoresistance (AMR). The impact of thermal fluctuations is also analyzed by adopting a Monte Carlo treatment to account for the unavoidable stochasticity in the Néel-vector dynamics at nonzero temperatures. Further investigation reveals that the desired functionality to modulate the probability distribution of the stochastic switching can be achieved via the properties of the signal pulse, enabling potential applications beyond the conventional computing paradigm.

II. THEORETICAL MODEL

The specific structure under consideration is shown in Fig. 1(a). As stated briefly above, the main functional material (i.e., the AFM) is assumed to have a C_4 symmetry with an in-plane hard z axis. The resulting four stable states of the Néel vector **L** are taken to be along the $\pm x$ and $\pm y$ directions. Further, the presence of interfaces with heterogeneous materials is expected to break the symmetry such that the Néel-vector orientations in the in-plane (y) and the cross-plane (x) direction can become energetically inequivalent [12]. This additional asymmetry in the Néel-vector states (x vs y) can be engineered through the shape of the structure, as well as through the strain at the heterointerfaces between the layers. As schematically illustrated in Figs. 1(b) and 1(c), the inequality in the barrier heights (and thus the torque required for switching) can enable unique determination of the final Néel-vector state. The magnetization of the FM layer in contact is set along the hard z axis, inducing rotation of the Néel vector around it. A conducting nonmagnetic spacer is assumed between the AFM and FM layers to avoid the effect of exchange bias. The purpose of the interface with a semiconductor layer at the other end of the structure is to induce a Schottky-type rectifying junction to enable both electrical writing and electrical reading in a two-terminal pillar configuration. In the write process, the Schottky junction works as a barrier when a bias is applied, causing spin-polarized electrons injected from the FM layer to accumulate and thus inducing an effective torque for rotation of the Néel vector. In the case of readout, a reverse bias makes the barrier permeable to electrical conduction. Orientations of the Néel vector parallel and perpendicular to the direction of the current flow are expected to lead to substantially different values of the output conductance

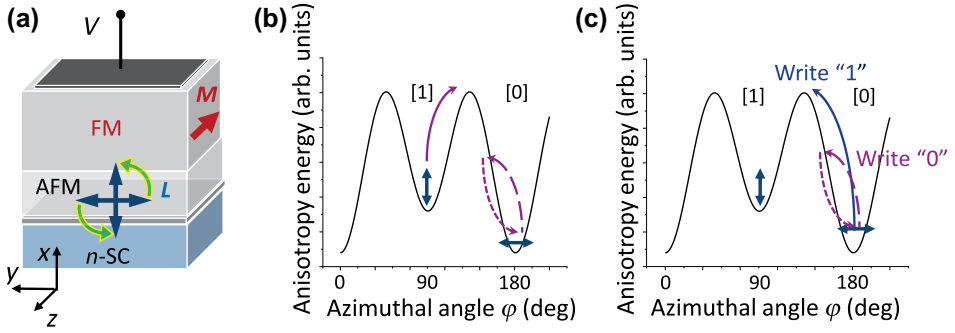

FIG. 1. (a) Schematic illustration of a two-terminal structure based on the spin-pumping effect. The easy axis of the FM layer is directed along the z direction, which corresponds to the hard axis of the tetragonal AFM. The double-ended arrows indicate the four equilibrium Néel-vector states. The interface with an n-type semiconductor (n-SC) forms a Schottky barrier. (b) Anisotropy-energy profile in the "easy" x-y plane (solid curve) in arbitrary units. The combination of the intrinsic C_4 symmetry of the AFM with the asymmetry of the structure induces an imbalance between the x (0° or 180°) and y (90°) directions. A bias pulse of moderate strength switches the Néel vector from the shallow state ("1") to the deeper state ("0") (solid arrow) but fails to induce a transition when starting from "0" (dashed arrows). (c) Envisioned write process. Following the initialization to state "0," a stronger pulse writes state "1," while a moderate pulse sets the Néel vector back to state "0." Hence the pulse strength can uniquely determine the final configuration.

through the phenomenon of AMR [13,14] or the tunneling variety of AMR (which tends to give a larger effect) [15]. A sizable bias can be used for robust detection without disturbing the Néel-vector state.

Our analysis of the response of the AFM to an effective-field pulse is based on the σ model of a collinear AFM, since the magnitude of the Néel vector $|\mathbf{L}|$ can be maintained essentially unchanged throughout all stages of evolution owing to the strong interlayer exchange interaction [16]. Accordingly, the actual variables used are the polar and azimuthal angles θ, φ of the unit vector $\mathbf{n} = \mathbf{L}/|\mathbf{L}| = (\sin\theta\cos\varphi, \sin\theta\sin\varphi, \cos\theta)$. In this treatment, the expression for the anisotropy energy of the structure shown above in Fig. 1(a) is written as

$$W(\mathbf{n}) = \frac{1}{2}K_{\parallel}n_z^2 - \frac{1}{2}K_2 n_x^2 - \frac{1}{4}K_4(n_x^4 + n_y^4), \qquad (1)$$

where $K_{\parallel}$ establishes the hard z axis, K_4 denotes the intrinsic C_4 anisotropy in the x-y plane, and K_2 specifies the additional contribution induced by the shape, interfacial strain, etc. The corresponding Lagrangian of the system, including the dissipation function, yields a set of second-order differential equations that are quite interdependent. However, as has been shown earlier [17,18], these equations for θ and φ can be decomposed provided the magnetic field affects the AFM along the hard z axis [i.e., $\mathbf{H} = (0, 0, H)$] and the initial states lie in the easy plane, which corresponds to the present conditions shown in Fig. 1. In this case, one solution for the polar angle, $\theta(t) = \pi/2$, remains stable in the subsequent evolution of the azimuthal angle $\varphi = \varphi(t)$. Thus, the transition of the Néel vector between the stable states essentially takes place in the x-y plane by overcoming a potential barrier of $\frac{1}{8}K_4 \pm \frac{1}{4}K_2$, depending on the initial orientation.

For a systematic analysis, it is convenient to introduce the dimensionless variables $t \to \omega_r t$ for time and $\mathbf{h} = \gamma\mathbf{H}/\omega_r$ for the magnetic field, where γ denotes the gyromagnetic ratio and $\omega_r = \gamma\sqrt{2H_{\mathrm{ex}}H_{\mathrm{an}}}$ is the frequency of the intrinsic resonance of the AFM, with an exchange field H_{ex} and an anisotropy field $H_{\mathrm{an}} = K_4/M_L$. M_L represents the sum of the absolute values of the sublattice magnetizations. By following the formalism developed in Ref. [18], the equation for the azimuthal angle can then be reduced to a canonical form

$$\ddot{\varphi} + 2\lambda\dot{\varphi} + \frac{\zeta}{2}\sin 2\varphi + \frac{1}{4}\sin 4\varphi = \dot{h}_{\mathrm{eff}} + \dot{h}_{\mathrm{th}}, \qquad (2)$$

where the conventional notation is used for the time derivatives $\dot{\varphi} = d\varphi/dt$, $\ddot{\varphi} = d^2\varphi/dt^2$, etc. The first term on the left-hand side accounts for the kinetic energy responsible for the inertial motion of the Néel vector, whereas the second term describes the dissipation by the damping parameter λ, which is directly related to the line width δ_r of the resonance of the AFM (equal to $\lambda\omega_r$). The two remaining contributions represent the anisotropy energy of the four potential wells discussed earlier in Eq. (1). The term $\frac{1}{4}\sin 4\varphi$ arises from the intrinsic anisotropy of the AFM, while the factor $\zeta = K_2/K_4$ in the third term signifies the relative importance of the symmetry reduction via the extrinsic factors ($C_4 \to C_2$). The right-hand side of Eq. (2) describes the torques due to the driving effective field h_{eff} and the fluctuating thermal field h_{th}. The origin of h_{eff} is the exchange interaction of the sublattices of the AFM with spin-polarized electrons delivered from the FM spin filter (i.e., the spin-pumping torque). As for h_{th}, the thermal fluctuations are directly related to the relaxation of the Néel vector via the fluctuation-dissipation theorem. The dependence on the time derivative shows clearly that a constant effective field does not contribute to the mechanism of switching from an energy minimum. This is apparent from the consideration that the torque induced by a constant field ($\mathbf{T}_F = \gamma\mathbf{H} \times \mathbf{n}$) cannot deliver energy to the system, due to its orthogonality with the resulting angular momentum (parallel to $\mathbf{H}$).

III. RESULTS AND DISCUSSION

The most prominent features of the Néel-vector dynamics under the influence of a spin-pumping torque can be captured by examining the case of an asymmetric driving pulse with a steep leading edge whose characteristic rise time is much shorter than the inverse resonance frequency, followed by a slow trailing edge. The situation mimics the dependence $\dot{h}_{\mathrm{eff}} = h_0\delta(t)$, where h_0 corresponds to the pulse amplitude. Since this approximation essentially sets the right-hand side of Eq. (2) to zero for $t > 0$ (h_{th} is not considered for the time being), the torque appears as the initial condition $\dot{\varphi}(0) = h_0$. Starting with an appropriate strength of h_0 above the threshold, the applied torque is capable of rotating the Néel vector between the x and y directions (states "0" and "1," respectively) in the course of its inertial motion. The numerical solutions clearly illustrate switching into the desired states, depending on the strength of h_0 (Fig. 2). As expected, a stronger pulse is needed to drive the Néel vector out of the deeper well (state "0"). In the case when the pulse is too strong (e.g., above the range for writing "1"), the induced torque can rotate the Néel vector by more than the desired 90°, eventually causing it to settle into state "0" (i.e., a 180° reversal). The upper bound on h_0 is set to prevent such occurrences in deterministic switching between states "0" and "1." A larger anisotropy factor ζ increases the difference in the two energy-barrier heights, resulting in an increased range of values of h_0 that set the final configuration to state "0" (the deeper well).

Since the electrical bias applied to the two terminals supposedly induces the necessary effective magnetic field, it is important to examine the magnitude of h_0 that can be practically achieved. For this, a capacitance analysis is used

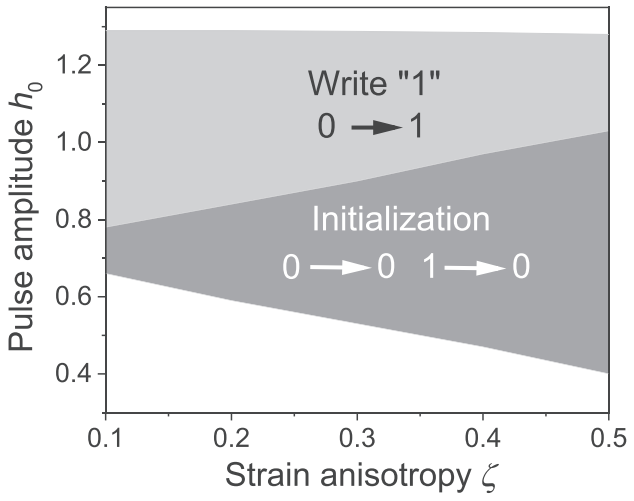

FIG. 2. Ranges of parameters h_0 (pulse amplitude) and ζ (strain anisotropy) for realizing initialization in state "0" (dark gray) and writing to state "1" (light gray). The results are obtained with a single steplike signal pulse. Thermal fluctuations are not considered. Both h_0 and ζ are normalized so that they are expressed in dimensionless units.

to obtain an expression for h_0 in terms of typical parameters of the structure. As the potential drop occurs mainly at the AFM/semiconductor interface, the primary contribution comes from the capacitance of the Schottky barrier, which can be given as $C = (\epsilon q N_d/V_d)^{1/2}$ per unit area [19]. Here, ϵ is the dielectric constant of the semiconductor, q is the unit charge, N_d is the doping density, and qV_d is the Schottky-barrier height. When a reverse bias V (equal to $-U_0$) is applied, excess electrons are injected from the FM layer into the AFM/semiconductor interface with a density $n_e = U_0 C/q$. As only a fraction η of these spin-polarized electrons mediate the effective exchange field, the result is

$$H_0 = \frac{\eta n_e J \Omega_0}{\gamma \hbar d_{\mathrm{AFM}}}, \tag{3}$$

which is averaged over the AFM thickness d_{AFM}. Here, J is the strength of the s-d exchange interaction, and Ω_0 denotes the volume of the primitive cell. Assuming the values $\epsilon = 11$, $N_d = 10^{19}$ cm^{-3}, and $qV_d = 0.5$ eV, a reverse bias of $U_0 = 300$ mV induces an excess electron density of about $n_e = 2.4 \times 10^{12}$ cm^{-2}. This yields $H_0 = 2.5$ T in an AFM of thickness $d_{\mathrm{AFM}} = 3$ nm with $\eta = 0.4$, $J = 0.7$ eV, and $\Omega_0 = 2 \times 10^{-22}$ cm^3. The corresponding angular velocity γH_0 of 4.4×10^{11} s^{-1} gives roughly h_0 $(= \gamma H_0/\omega_r) \sim 1$, as ω_r is typically in the range of approximately 10^{11}–10^{12} s^{-1} in an AFM.

For a more specific example, the material parameters of the commonly used bimetallic alloy MnPt are adopted for a numerical estimate. As desired, MnPt has tetragonal symmetry and is quite sensitive to structure-induced magnetic anisotropy [12]. The relatively weak in-plane anisotropy in MnPt (see Refs. [20–22]) suggests that K_4 and ω_r are around 10^5 erg/cm^3 and 4.9×10^{11} s^{-1} (i.e., $1/\omega_r \simeq 2$ ps), respectively. These values indicate that a U_0 of 330 mV is sufficient to generate a dimensionless amplitude $h_0 = 1$ in a FM/MnPt/n-Si structure. With the parameters specified above, the energy required for 90° switching is estimated to be in the tens of attojoules for an AFM of sufficiently large dimensions (i.e., with a sufficiently large total anisotropy energy) to ensure nonvolatile operation at room temperature. These estimates are used in the subsequent analysis.

The results discussed thus far do not explicitly account for the effect of random thermal fields. As such, the outcome of the antiferromagnetic dynamics is determined solely by the input signal, without any uncertainty or stochasticity (see, for example, Fig. 2). In reality, however, thermal fluctuations not only control the spontaneous transitions from the potential wells but also affect the switching dynamics, leading to a probabilistic description, particularly in the vicinity of threshold conditions. The contribution of the fluctuating field $h_{\mathrm{th}}(t)$ can be considered by simply adding the fieldlike torque $(d/dt)h_{\mathrm{th}}(t)$ to the right-hand side of Eq. (2). Because of the explicit dependence on the time derivative, the conventional approximation based on a series of random step functions for white noise cannot be applied to the antiferromagnetic dynamics [23]. As an alternative, a spectral representation is adopted in the form of a Fourier-series expansion with random amplitudes [18]. Here, the broadening δ_r of the resonant frequency (or the inverse relaxation time τ_m^{-1}) offers a physical basis for discretization of the spectral domain into comparable intervals, since the response of a damped Néel-vector motion becomes practically invariant with respect to a perturbative frequency swing in the range of δ_r due to the broadening. In other words, the response of the AFM to thermal noise is virtually equivalent to a series of sinusoidal perturbations with random amplitudes and frequencies $n\delta_r$ $(n = 1, 2, \ldots)$. An upper bound on the sum N can also be introduced by considering the finite autocorrelation time τ_c, where N can be estimated as τ_m/τ_c. Finally, the fluctuation-dissipation theorem determines the amplitudes of the fluctuating field components in the form (see Ref. [18] for additional details)

$$h_{\mathrm{th}}(t) = \lambda \left(\frac{2k_{\mathrm{B}}T}{NK_4V}\right)^{1/2} \left(\sum_{n=1}^{N} \alpha_n \sin n\lambda t + \sum_{n=1}^{N} \beta_n \cos n\lambda t\right), \tag{4}$$

where the time t is in dimensionless units and $(1/2N)\sum_{n=1}^{N}\langle \alpha_n^2 + \beta_n^2 \rangle = 1$. This expression clearly produces the derivative $(d/dt)h_{\mathrm{th}}(t)$ in the form of a smooth function that can be directly incorporated into Eq. (2).

Since the noise expression given above applies only for a duration up to τ_m due to relaxation, a time period longer than this interval requires repeated random selections. Moreover, each switching event necessitates independent consideration to ensure an accurate description of its stochastic nature, whose probability distribution can be obtained by a Monte Carlo treatment. Evidently, the resulting probability distribution depends also on the properties of the input signal, such as the pulse strength h_0. In the actual computation, Eq. (2) is solved numerically for each time step τ_m under the specified conditions (e.g., $h_{\rm eff}$) along with a set of Fourier amplitudes α_n and β_n selected randomly for the given period. This process is continued in time until the simulation concludes. Then, the entire calculation is repeated for a sufficient number of iterations to establish accurate statistics (i.e., of successful versus unsuccessful events) for the desired probability distribution function.

Figure 3 shows the calculated switching probability (for "1" → "0") as a function of h_0 for different AFM sizes. The dashed line represents the deterministic case, where random thermal fields are not considered. Accordingly, the 90° Néel-vector rotation occurs with 100% certainty in this case if h_0 is even slightly above the threshold. The resulting probability distribution has a step-function form. In contrast, thermal fluctuations broaden the distribution so that it has a finite slope, as expected. It is interesting to note that the best fit to the calculated probability distribution can be expressed in terms of the Gaussian error function erf(x) [24] as

$$P(h_0) = \frac{1}{2} + \frac{1}{2}\,\mathrm{erf}\left(\frac{h_0 - h_\zeta}{\sqrt{2}\sigma}\right). \tag{5}$$

The standard deviation σ at a finite temperature is directly related to the geometry of the structure, while the critical field h_ζ depends on the anisotropy factor ζ. For cases with AFM dimensions of $10 \times 10 \times 3$ nm^3, $25 \times 25 \times 3$ nm^3, and $65 \times 65 \times 3$ nm^3, this estimate gives standard deviations of 0.18, 0.11, and 0.05, respectively (or 60, 36, or 16 mV in the units of the bias voltage). The value of h_ζ is fixed at 0.53 in all three cases (see also the dashed line). Needless to say, large AFMs are less susceptible to thermal fluctuations with respect to random switching. A similar picture arises in the case of "0" → "1" switching, with threshold behavior around $h_\zeta \simeq 0.83$. Compared with the case in Fig. 3, however, the dispersion of the successful events (i.e., the standard deviation) becomes narrower, since the stronger pulse amplitude diminishes the impact of thermal fluctuations. As such, this case may not be as desirable when the focus is to exploit its probabilistic applications and control.

The significance of these results can be far more prominent if electrical control of σ can be achieved dynamically rather than via the geometry of the structure. One such

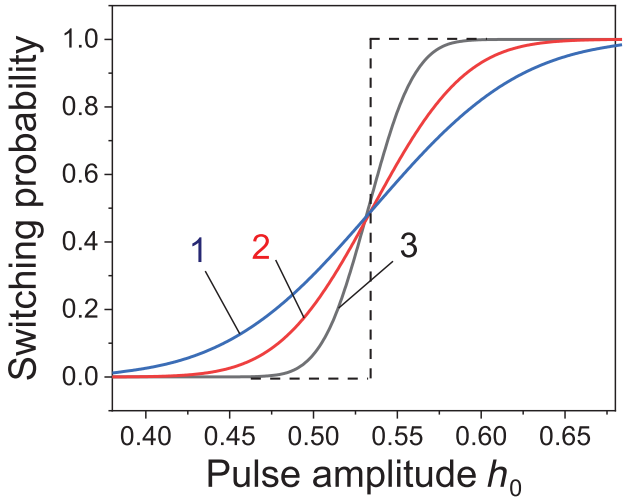

FIG. 3. Switching probability versus pulse amplitude calculated in the presence of thermal fluctuations at room temperature with $\zeta = 0.3$ and $\lambda = 0.2$ (for "1" → "0"). A single step-function signal pulse is assumed. Curves 1, 2, and 3 correspond to AFM dimensions of $10 \times 10 \times 3$ nm^3, $25 \times 25 \times 3$ nm^3, and $65 \times 65 \times 3$ nm^3, respectively. The dashed line shows the deterministic switching in the absence of thermal fields (or in the limit of very large size with $h_\zeta = 0.53$). As stated in the text, the pulse amplitude is in dimensionless units.

example is provided by probabilistic computing [25,26]. To examine this possibility, a more complete expression is considered for the input effective field $h_{\rm eff}(t)$ (or bias). Instead of a step-function-like form, the pulse front is described more accurately by the rise time τ_1 and the electron spin-flip relaxation time T_1 as $h_1(t) = h_0(1 - e^{-t/\tau_1})e^{-t/T_1}$. Then, assuming that the input bias is turned off after a duration Δt, the falling edge of the effective field (at $t \geq \Delta t$) can be written similarly as $h_2(t) = [h_1(\Delta t) - h_0(1 - e^{-(t-\Delta t)/\tau_2})]e^{-(t-\Delta t)/T_1}$. Here, the second part of the expression describes the depletion of carrier spins via discharging through the FM spin filter (with a characteristic time τ_2). Apparently, the step-function approximation corresponds to the case of $\tau_1 \ll 1$ and long τ_2, Δt, and T_1.

Among the parameters that determine $h_{\rm eff}(t)$, our analysis is focused on the pulse amplitude h_0 and the duration Δt, since these can be modulated dynamically as desired. In addition to the amplitude, the pulse duration also affects the Néel-vector dynamics, which is apparent from the expression for $h_2(t)$. For instance, a reduction in Δt tends to enhance the impact of the falling edge, which countermands the initial torque induced by the pulse front. This may not only shift the critical value h_ζ but also provide an environment where the influence of thermal fluctuations can manifest itself prominently in the Néel-vector dynamics. Figure 4 shows the probability distribution calculated as a function of h_0 for three different values of Δt. Indeed, a shorter pulse duration tends to require a

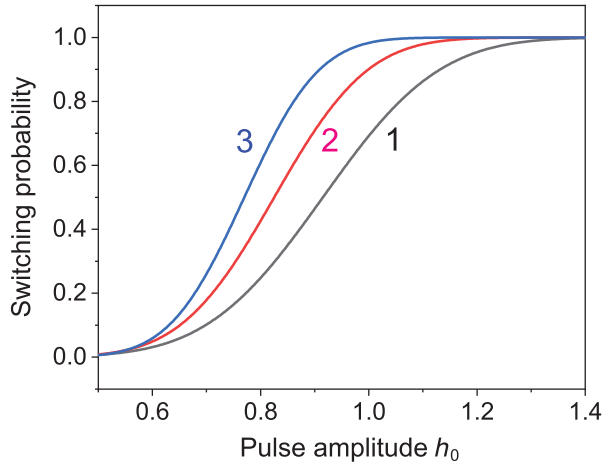

FIG. 4. Switching probability versus pulse amplitude calculated in the presence of thermal fluctuations at room temperature for three different values of the pulse duration (for "1" → "0"). Specifically, curves 1, 2, and 3 correspond to Δt values of 2, 3, and 5 (or 4, 6, and 10 ps, respectively, for a MnPt structure of dimensions $65 \times 65 \times 3$ nm^3). The parameters used are $\tau_1 = 0.5$, $\tau_2 = 5$, $T_1 = 5$, $\zeta = 0.3$, and $\lambda = 0.2$. The pulse amplitude h_0 is also in dimensionless units.

stronger pulse strength to achieve the same level of switching, leading to a more gradual line shape. Assuming the typical parameters $\tau_1 = 0.5$, $\tau_2 = 5$, $T_1 = 5$, $\zeta = 0.3$, and $\lambda = 0.2$, the estimated standard deviation σ is shown to be 0.14, 0.11, and 0.09 for Δt values of 2, 3, and 5 (e.g., 4, 6, and 10 ps, respectively, for a MnPt structure of dimensions $65 \times 65 \times 3$ nm^3). The corresponding h_ζ gives 0.91, 0.82, and 0.77, respectively. The electrical bias can clearly modulate the probability distribution function rather substantially, as anticipated. Note that a trade-off may need to be made between nonvolatility and the thermally induced range of control of the probability distribution. The results obtained are qualitatively consistent with experimentally observed stochastic switching in a FM via the STT [25]. AFM structures based on the spin-pumping torque are expected to offer significant advantages in terms of energy consumption and switching speed.

IV. SUMMARY

This study shows that both electrostatic control of Néel-vector states and their detection via AMR can be achieved in a pillar structure containing a metallic AFM with tetragonal symmetry by taking advantage of a Schottky junction with an adjacent semiconductor layer. In particular, the currentless spin-pumping torque originating from the exchange field of injected spin-polarized electrons can achieve the desired rotation with an operating energy that can be reduced to tens of attojoules. The additional structure-induced anisotropy facilitates selective localization of the Néel vector in a state either parallel or perpendicular to the pillar axis. Consideration of thermal fluctuations at finite temperatures affects the device performance, especially when the AFM layer is small. Moreover, the stochastic properties of the switching probability can be controlled by tailoring the input pulse in the electric bias. Compared with their FM-based counterparts, the fast dynamics makes AFM-based devices particularly attractive, as many more independent events can be evaluated in a given time duration (i.e., a faster computing speed is possible). Similar advantages are expected in terms of the energy requirement per operation, since the applied electrical signal can be much shorter. In addition, the absence of stray fields can allow high-density integration where this is not possible in FM multicell systems due to the long-range nature of the magnetic field (i.e., crosstalk). These characteristics are expected to make AFM-based structures a strong candidate for applications in nonvolatile memory and probabilistic computing.

ACKNOWLEDGMENTS

This work was supported, in part, by the US Army Research Office (Grant No. W911NF-16-1-0472).

[1] M. N. Baibich, J. M. Broto, A. Fert, F. Nguyen Van Dau, F. Petroff, P. Etienne, G. Creuzet, A. Friederich, and J. Chazelas, Giant Magnetoresistance of (001)Fe/(001)Cr Magnetic Superlattices, Phys. Rev. Lett. **61**, 2472 (1988).

[2] G. Binasch, P. Grünberg, F. Saurenbach, and W. Zinn, Enhanced magnetoresistance in layered magnetic structures with antiferromagnetic interlayer exchange, Phys. Rev. B **39**, 4828(R) (1989).

[3] J. C. Slonczewski, Current-driven excitation of magnetic multilayers, J. Magn. Magn. Mater. **159**, L1 (1996).

[4] L. Berger, Emission of spin waves by a magnetic multilayer traversed by a current, Phys. Rev. B **54**, 9353 (1996).

[5] A. Manchon, J. Železný, I. M. Miron, T. Jungwirth, J. Sinova, A. Thiaville, K. Garello, and P. Gambardella, Current-induced spin-orbit torques in ferromagnetic and antiferromagnetic systems, Rev. Mod. Phys. **91**, 035004 (2019).

[6] E. V. Gomonay and V. M. Loktev, Spintronics of antiferromagnetic systems, Low Temp. Phys. **40**, 17 (2014).

[7] T. Jungwirth, X. Marti, P. Wadley, and J. Wunderlich, Antiferromagnetic spintronics, Nat. Nanotechnol. **11**, 231 (2016).

[8] R. Cheng, M. W. Daniels, J.-G. Zhu, and D. Xiao, Ultrafast switching of antiferromagnets via spin-transfer torque, Phys. Rev. B **91**, 064423 (2015).

[9] A. S. Núñez, R. A. Duine, P. Haney, and A. H. MacDonald, Theory of spin torques and giant magnetoresistance in antiferromagnetic metals, Phys. Rev. B **73**, 214426 (2006).

[10] E. V. Gomonay and V. M. Loktev, Spin transfer and current-induced switching in antiferromagnets, Phys. Rev. B **81**, 144427 (2010).

[11] Y. G. Semenov and K. W. Kim, Spin pumping torque in antiferromagnets, Appl. Phys. Lett. **110**, 192405 (2017).

[12] I. J. Park, T. Lee, P. Das, B. Debnath, G. P. Carman, and R. K. Lake, Strain control of the Néel vector in Mn-based antiferromagnets, Appl. Phys. Lett. **114**, 142403 (2019).

[13] S. Yu. Bodnar, L. Šmejkal, I. Turek, T. Jungwirth, O. Gomonay, J. Sinova, A. A. Sapozhnik, H.-J. Elmers, M. Kläui, and M. Jourdan, Writing and reading antiferromagnetic Mn_2Au by Néel spin-orbit torques and large anisotropic magnetoresistance, Nat. Commun. **9**, 348 (2018).

[14] Q. Liu, H. Y. Yuan, K. Xia, and Z. Yuan, Mode-dependent damping in metallic antiferromagnets due to intersublattice spin pumping, Phys. Rev. Mater. **1**, 061401 (2017).

[15] B. G. Park, J. Wunderlich, X. Martí, V. Holý, Y. Kurosaki, M. Yamada, H. Yamamoto, A. Nishide, J. Hayakawa, H. Takahashi, A. B. Shick, and T. Jungwirth, A spin-valve-like magnetoresistance of an antiferromagnet-based tunnel junction, Nat. Mat. **10**, 347 (2011).

[16] B. A. Ivanov, Mesoscopic antiferromagnets: Statics, dynamics, and quantum tunneling, Low Temp. Phys. **31**, 635 (2005).

[17] R. Khymyn, I. Lisenkov, V. Tiberkevich, B. A. Ivanov, and A. Slavin, Antiferromagnetic THz-frequency Josephson-like oscillator driven by spin current, Sci. Rep. **7**, 43705 (2017).

[18] Y. G. Semenov, X. Xu, and K. W. Kim, Thermal fluctuations in antiferromagnetic nanostructures, J. Magn. Magn. Mater. **489**, 165457 (2019).

[19] E. H. Rhoderick and R. H. Williams, *Metal-Semiconductor Contacts* (Clarendon, Oxford, 1988), 2nd ed.

[20] H. Hama, R. Motomura, T. Shinozaki, and Y. Tsunoda, Spin–flip transition of $L1_0$-type MnPt alloy single crystal studied by neutron scattering, J. Phys.: Condens. Matter **19**, 176228 (2007).

[21] Z. Lu, R. V. Chepulskii, and W. H. Butler, First-principles study of magnetic properties of L1(0)-ordered MnPt and FePt alloys, Phys. Rev. B **81**, 094437 (2010).

[22] T. Oda, I. Pardede, T. Kanagawa, N. Ikhsan, D. Yoshikawa, and M. Obata, Shape magnetic anisotropy from spin density in nanoscale slab systems, IEEE Tran. Magn. **55**, 1300104 (2019).

[23] V. D. Tsiantos, T. Schrefl, W. Scholz, and J. Fidler, Thermal magnetization noise in submicrometer spin valve sensors, J. Appl. Phys. **93**, 8576 (2003).

[24] This fit with a Gaussian error function is of an empirical nature. The physical origin of the functional shape is unclear.

[25] J. Grollier, D. Querlioz, and M. D. Stiles, Spintronic nanodevices for bioinspired computing, Proc. IEEE **104**, 2024 (2016).

[26] D. Pinna, F. Abreu Araujo, J.-V. Kim, V. Cros, D. Querlioz, P. Bessiere, J. Droulez, and J. Grollier, Skyrmion gas Manipulation for Probabilistic Computing, Phys. Rev. Appl. **9**, 064018 (2018).